

# An improved rheology model for the description of the rate-dependent cyclic behavior of high damping rubber bearings



D.A. Nguyen<sup>a,\*</sup>, J. Dang<sup>a</sup>, Y. Okui<sup>a</sup>, A.F.M.S. Amin<sup>b</sup>, S. Okada<sup>c</sup>, T. Imai<sup>d</sup>

<sup>a</sup> Department of Civil and Environmental Engineering, Saitama University, Saitama 338-8570, Japan

<sup>b</sup> Department of Civil Engineering, Bangladesh University of Engineering and Technology, Dhaka 1000, Bangladesh

<sup>c</sup> Civil Engineering Research Institute for Cold Region, PWRI, Sapporo 062-8602, Japan

<sup>d</sup> Rubber Bearing Association, Tokyo 107-0051, Japan

## ARTICLE INFO

### Article history:

Received 24 October 2014

Received in revised form

5 June 2015

Accepted 8 June 2015

Available online 17 July 2015

### Keywords:

High damping rubber bearings

Rate dependence

Low temperature

Rheology model

Parameter identification

## ABSTRACT

An improved rheology model, inspired from explicit experiments is conceived to represent rate-dependent cyclic shear behavior of high damping rubber bearings at subzero and room temperatures. Total stress has been decomposed into nonlinear rate independent elasto-plastic stress, nonlinear elastic stress and nonlinear visco-elasto-plastic overstress branches. To represent nonlinear viscosity behavior, 'overstress branch' has been generalized by putting linear elastic spring in parallel to nonlinear elasto-plastic model, placed in series with nonlinear dashpot. Constitutive relations for model elements have been designated for respective fundamental phenomenon observed in constant strain rate experiments. An optimum calculation approach is developed to determine a unique set of overstress parameters capable not only of representing constant strain rate cyclic tests but also sinusoidal tests with variable input strain rates. Essential abilities of the proposed model and adequacy of estimated parameters have been confirmed by comparing numerical simulation results with experiments conducted at  $-30\text{ }^{\circ}\text{C}$ ,  $-10\text{ }^{\circ}\text{C}$  and  $23\text{ }^{\circ}\text{C}$ .

© 2015 Elsevier Ltd. All rights reserved.

## 1. Introduction

Application of laminated rubber bearings as base isolation devices [1,2] got wider acceptance in Japan after promising field level performances in 1995 Kobe Earthquake. To introduce energy dissipation properties within the bearing device, lead rubber bearing (LRB) was developed in New Zealand [3,4] with lead plugs installed inside laminated natural rubber bearings (RB). High damping rubber (HDR) later emerged as a novel material for such bearing devices not only to eliminate the necessity of installing lead plugs inside RB but also to enhance energy dissipation properties compared to LRB. A more recent concern over the reduction of energy dissipation property per cycle in LRB due to self-heating of lead plug upon cyclic loading [5,6] is also questioning the capability of LRB in long duration earthquakes, for example 2011 Tohoku earthquake. The innovation of HDR led to a wide adoption of high damping rubber bearings (HDRBs) as visco-elasto-plastic dampers in next generation base isolated structures all over the world (Fig. 1). In contrast to LRB, where rate dependence effect is much less significant even for low temperature cases [3,7], however, even after years of practice, some of the

very important mechanical behaviors of HDR, such as the rate or temperature dependent behaviors are still difficult and less understood issues in engineering practice [8]. Yet, development of an advanced rheology model of HDRBs for designing base isolated structures in cold weather conditions and more general dynamic loading cases is much warranted. Nevertheless, any effort in this direction shall be founded on basic understanding of constitutive properties of HDRBs observed under low temperature test conditions.

Fundamental nonlinear elastic and nonlinear viscosity behaviors of HDR at room temperature are known from the observations reported in Amin et al. [9–11]. Contemporary experimental observations [12,13] on laminated rubber bearings also show that restoring force–displacement loops of HDRBs depend prominently on loading history and strain level. Hysteresis loops of HDRBs were further observed to strongly depend on loading rate, ambient temperature and even time interval between two loading tests. Bhuiyan et al. [14] reviewed well-known constitutive behaviors of HDR and their effects on the mechanical behavior of HDRBs. Past efforts on developing analytical representation of room temperature mechanical behaviors in rate dependent and rate independent rheology models were also summarized there. Subsequently, Bhuiyan et al. [14] extended the Maxwell model (Elements C and D, Fig. 2) by adding a nonlinear elastic spring (Element B) and an elasto-plastic model (spring-slider, Element A and S) in parallel to

\* Corresponding author. Tel.: +81 48 858 3558; fax: +81 48 858 3558.

E-mail address: [dungsaitama@gmail.com](mailto:dungsaitama@gmail.com) (D.A. Nguyen).

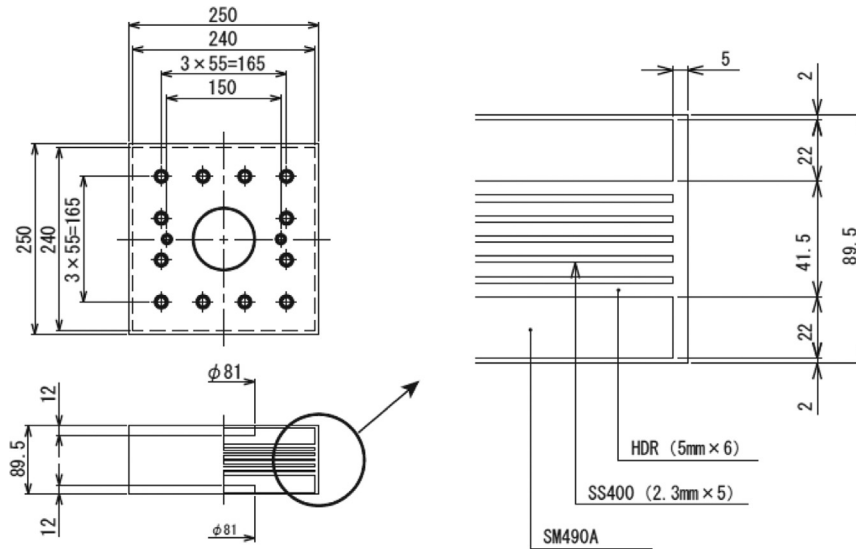


Fig. 1. Size of Type A specimen following the ISO standard ([31]) [mm] for room temperature tests.

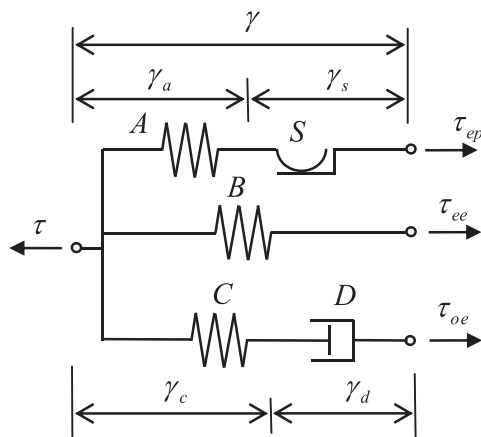


Fig. 2. Rheology model of HDRBs showing stress and strain decompositions for room temperature behavior. (after [14]).  $\tau$ : average shear stress,  $\gamma$ : average shear strain,  $\tau_{ee}$ : nonlinear elastic response,  $\tau_{ep}$ : elasto-plastic response,  $\tau_{oe}$ : overstress due to viscosity,  $\tau = \tau_{ep}(\gamma_a) + \tau_{ee}(\gamma) + \tau_{oe}(\gamma_c)$ .

represent a set of phenomena observed in full scale tests on HDRBs. The overstress ( $\tau_{oe}$ ) branch was modeled with a linear spring (Element C) added in series with a nonlinear dashpot (Element D). In order to identify constitutive relations of each element in the rheology model, in line with the concepts followed in Lion [15] and Amin et al. [9,10] on natural rubber (NR) and HDR, an experimental scheme comprised of three types of tests at constant strain rates, namely cyclic shear (CS) tests, multi-step relaxation (MSR) tests and simple relaxation (SR) tests were carried out at room temperature on HDRBs specimens with the standard ISO geometry. To observe the fundamental viscosity behaviors during loading and unloading, MSR tests contained multiple hold times while SR tests contained a single hold time during loading and unloading. More recently, Yamamoto et al. [16] investigated the nonlinear behavior of HDRBs under horizontal bidirectional loading at room temperature and propose an analytical model. However, no effort is known either to investigate the applicability of the existing rheology models or to propose a new model for simulating the low temperature behavior of HDRBs. Kato et al. [17] very recently proposed analytical Model for elastoplastic and creep-like room temperature behavior of HDRB.

Effect of temperature on visco-elasto-plastic phenomena in rubber is a much less investigated topic reported in current literatures. The effect of ambient temperature and the exposure history on constitutive behavior of rubber is addressed in Lion [18] and Fuller et al. [19]. A recent comprehensive review of literature together with experimental observations on natural rubber-polybutadiene rubber (NR/BR) blend is provided in Amin et al. [20]. In these studies; rate dependence, hysteresis and well-known Mullins' effect [21] were critically addressed for temperature dependence. Depending on the type and composition of the rubber, the mechanical behavior was found to be affected strongly by ambient temperature, often by temperature history and less often by the loading history. Generally, rubbers tested at lower temperatures have shown larger rate dependence, hysteresis and Mullins' effect whereas these effects got gradually diminished at temperatures above the room temperature. Furthermore, Fuller et al. [19] reports temperature history dependence of HDR due to crystallization effect on prolonged exposure to low temperature and associated increase in shear modulus. Amin et al. [20] emphasizes on the role of loading history dependence due to fundamental Gough–Joule effect, determined by the entropy elasticity and inelastic energy dissipation or hysteresis on self-heating [22–24] of large rubber devices due to quasi-adiabatic mechanical process acting on it. The later notion therefore further emphasizes the importance of thermal boundary defined mostly by the specimen size on the response of bearings. Yet, no effort in this respect is known where the fundamental constitutive behaviors observed either in HDR or HDRBs at low temperatures is investigated. This obviously restricted not only the development of a rheology model for HDRBs for seismically active cold region applications for example, Hokkaido, Japan (1968 Tokachi Earthquake) and Alaska, USA (1964 Alaska Earthquake) but also the performance prediction of existing structures in those regions.

The feat of a rheology model developed to represent a device in structural analysis is frequently judged by its ability to simulate not only the fundamental constitutive behaviors but at least also in simulating some practical loading histories that a designer would use at the design desk. Furthermore, the size of test specimen and its role on self-heating effect upon cyclic loading needs to be critically addressed at least to generate plausible conclusions on the limits of real ability of a model. In the past, this came out to be truer for HDR than other rubber-like materials when more and more test information on the former became sequentially

available. The elasticity parameters and the hyperelasticity model proposed in Amin et al. [9] for monotonic compression was revisited to include monotonic shear regime deformations in Amin et al. [10]. The nonlinear viscosity effects for monotonic compression and shear regimes were modeled and identified in Amin et al. [11]. On the other hand, Bhuiyan et al. [14] proposed a rheology model to represent the cyclic behaviors but only at room temperature. Though a characterization scheme for nonlinear viscosity effect could be presented there in details, it was not possible to provide any illustrative information over there about adherence of the model in representing fundamental constitutive behaviors e.g. equilibrium response and instantaneous response. Furthermore, the model had to use two different sets of parameters to represent CS responses under constant input strain rate and under variable input strain rate e.g. when the bearings are subjected to sinusoidal loading. All these shortcomings obviously indicate the necessity of addressing not only the low temperature behavior but also proposing a scheme to identify optimal parameters at least to hold for both constant strain rate loading and sinusoidal loading cases. Any effort in such direction should be a bit challenging in the sense when there are the difficulties of performing long duration tests of standard size rubber bearings with reproducible accuracy not only under subzero thermal equilibriums but also under sufficiently high strain rates (CS, MSR and SR tests) together with inclusion of hold times in input strain history (e.g. MSR and SR tests). Due to the general shortcomings of existing knowledge-base, design and analysis for structures with laminated rubber base isolation devices, design code and specifications [25–28] still generally recommend use of simplified bilinear elasto-plastic models, to represent the restoring force-displacement relationship of laminated rubber bearings by omitting rate dependent behavior of HDRBs.

The literature investigations conducted by some authors [12–14] have shown that the mechanical behavior of HDRBs demonstrate strong nonlinearity in rate-dependency property at room temperature. In addition, the experimental observations in [18,20] have indicated that the rate-dependent viscosity properties of HDRBs increase at low temperatures. Therefore, a rate-dependent model is indispensable for HDRBs, especially at low temperatures. The experimental investigations in [29] have shown that the variation of the equivalent stiffness and the equivalent damping ratio of HDRBs were small at higher room temperatures, while this variation is very large at low temperatures. On the basis of these investigations, the test temperatures are selected at room and low temperatures.

With these backgrounds, in this study, a test program was carried out to investigate the rate-dependent hysteresis behavior of HDRBs at room (23 °C) and also at low temperatures (−10 °C and −30 °C). An extended rheology model and a parameter identification scheme are proposed to represent the rate dependent hysteresis behavior reliably for HDRBs. Finally, the ability of the proposed model and parameter identification procedure are verified by comparing the numerical simulation results and loading histories with constant strain rates (with or without hold times) and variable strain rates for each of the three reference thermal equilibriums for HDRBs.

## 2. Strain-rate effect in HDRBs under cyclic loading

### 2.1. Specimens and test set-up

Tests at room and low temperatures were conducted in this study following same test protocols and same HDR materials as presented in Bhuiyan et al. [14]. All specimens had square cross-section. The dimensions and material properties of the specimens

are given in Table 1. Results for room temperature experiments follow from Bhuiyan [30] and Bhuiyan et al. [14] indicated there as HDR3. These specimens follow ISO standard [31] and marked as Type A (Fig. 1). Low temperature tests reported in this study were performed on specimens having smaller dimension and marked as Type B. Use of smaller specimens are beneficial in maintaining uniform temperature all over the specimen closer to low ambient temperatures by overcoming the self-heating effect usually observed upon cyclic loading in large rubber bearings [32]. Such interference on the observed responses is more critical for low temperature cases [20]. Moreover, the stiffness of HDRBs is very high at low temperatures. Type B specimens with smaller dimensions are suitable with the capability of the test machine in delivering very high force to attain the target strain at a very high strain rate. Geometric details of Type A and Type B specimens are illustrated in Figs. 1 and 3.

All tests were conducted with new specimens. A computer-controlled servo-hydraulic testing machine capable of delivering appropriate displacement histories at a prescribed rate was installed inside a walk-in type large environmental test chamber as shown in Fig. 4. To ensure homogeneous temperature distribution, the specimen was first let in the temperature chamber at room temperature (23 °C or above) and allowed to cool down under load-free conditions. During this process, the specimen inside the chamber was allowed to change dimensions under stress-free condition. After attaining the test temperature for the particular test, the specimen to be tested was kept inside the test chamber for more 24 h to equilibrate the temperature inside the specimen. In order to take the effect of axial load into account, all specimens were tested under shear deformation with a constant vertical compressive average stress of 6 MPa. This value is selected based on the data in [33]. The loading program including new tests in this study and those already presented in Bhuiyan [30] and Bhuiyan et al. [14] are shortly described in Table 2.

### 2.2. Test protocols to explore the rate dependency behavior in preloaded specimens

HDRBs specimens were subjected to four cyclic loading protocols, namely, multi-step relaxation (MSR) tests, cyclic shear (CS) tests, sinusoidal loading (Sin) tests, and simple relaxation (SR) tests at −30 °C, −10 °C and 23 °C. Figs. 5 and 6 illustrate the applied strain histories on the specimens for MSR tests, SR tests, CS tests and Sin tests at different temperatures. As seen in Fig. 5, MSR tests are cyclic loading tests that were conducted at a constant strain rate of 5.5/s at each loading step but after a small part of shear strain application, the specimen was kept on hold at that particular shear strain for 1200 s to let the stress in HDRBs to relax to its equilibrium state (Fig. 5). A number of relaxation periods (hold times) were applied as shown in the figure. SR tests are carried out in a fashion similar to MSR tests but with only single hold time (1800 s) between loading and unloading. SR tests performed at three shear strain levels e.g. 1.00, 1.50, 1.75 provide information about the rate dependent behavior induced by viscosity in specimens at respective strain levels (Fig. 5(c)). CS tests loaded the specimens under three different loading rates e.g. 1.5/s, 5.5/s, and 8.75/s, to investigate the rate dependent behavior (Fig. 6). Loading rate of 8.75/s is a very high value for an isolation device. It was set as “*extremely fast*” to observe the upper limit of rate dependent state [9], mentioned as instantaneous state at the rest of this paper. Sinusoidal tests are conducted in this study with a strain rate amplitude of 5.5/s (Fig. 6(c)). Virgin rubber exhibits a well-known stress-softening phenomenon, referred to as Mullins effect [21], in the first loading cycle. In order to remove Mullins effect, all virgin specimens were first subjected to a preloading sequence before the actual tests [9–11,14,18]. The preloading

consisted of 6 sinusoidal loading cycles at 1.75 strain level amplitude and 0.05 Hz frequency. The applied maximum strain in preloading was 2.50 for MSR tests.

The measured shear force and displacement are normalized to average shear stress and strain. Average shear stress, throughout this essay is calculated as the ratio  $\tau$  and the average shear strain  $\gamma$  are calculated by following equations.

$$\tau = \frac{F}{Q} \tag{1}$$

$$\gamma = \frac{u}{h} \tag{2}$$

where,  $F$  is the horizontal shear force;  $Q$  is the area of the cross-section of the bearings;  $u$  is the horizontal displacement and  $h$  is the total rubber thickness (Table 1). Rate dependent behaviors observed in these loading tests are summarized in following sections.

2.3. Equilibrium hysteresis behavior from MSR tests

The equilibrium state stress–strain responses of HDRBs can only be obtained by applying an infinitely slow loading rate which is difficult in practice [14,34]. Therefore, MSR tests were suggested in the past to identify the equilibrium state behavior at different

temperatures (Fig. 5). Stress histories recorded in MSR tests at three different temperatures are plotted in Fig. 7. It is seen that the stress value drops once the applied strain was on hold. In general, the magnitude of stress relaxation for a particular applied strain level, perceived as the difference between the peak stress (beginning of hold time for a particular strain level) and end stress (end of hold time for particular strain level) is larger during loading than in unloading. Furthermore, from a comparison between the figures it is clear that the peak stress value recorded at beginning of hold time for a particular strain level is larger than that recorded at the respective strain level but at a lower temperature. Not to mention, all these general observations is indicative of the existence of rate dependence property in HDRBs but shall be carefully examined further for ruling out the strain history dependence properties via SR tests. This aspect is addressed in Section 2.4 and Section 2.5.

Nevertheless, at the end of each relaxation period, the stress attains to almost a stable state, and that converged value can be regarded as the equilibrium state of the device. The converged value of stress after a relaxation step is defined as an equilibrium stress. The shear stress–strain response in the equilibrium state can be traced by connecting all the equilibrium state points as illustrated in Fig. 8.

2.4. Stress relaxation behavior from SR tests

The relaxation behavior induced by viscosity property is examined by a series of SR tests at the three reference temperatures. In each of these tests, the stress relaxation responses are obtained from identical applied strain histories at a constant monotonic strain rate (5.5/s), whereas the only difference is the strain level that the specimen was subjected to immediately before the beginning of the hold time. Each test was carried out in three reference ambient temperatures (Fig. 5(c)).

The stress histories obtained from SR tests at different temperatures and shear strain levels are plotted in Fig. 9. In the plots, the initial stresses at the beginning of the hold time (relaxation period) are seen to be strongly temperature-dependent. This behavior can be attributed to the temperature dependence of the viscosity property of HDRBs. The value of stress seen to get reduced gradually during the hold time is known as the classical

Table 1 Dimension and material properties of HDR bearing specimens.

Particulars	Specifications	
	Type A	Type B
Cross-section (mm <sup>2</sup> )	57,600 mm <sup>2</sup> , 240 mm × 240 mm	25,600 mm <sup>2</sup> , 160 mm × 160 mm
Number of rubber layers	6	5
Thickness of one rubber layer (mm)	5	4
Total rubber thickness $h$ (mm)	30	20
Thickness of one steel plate (mm)	2.3	2.3
Nominal shear modulus (MPa)	1.2	1.2

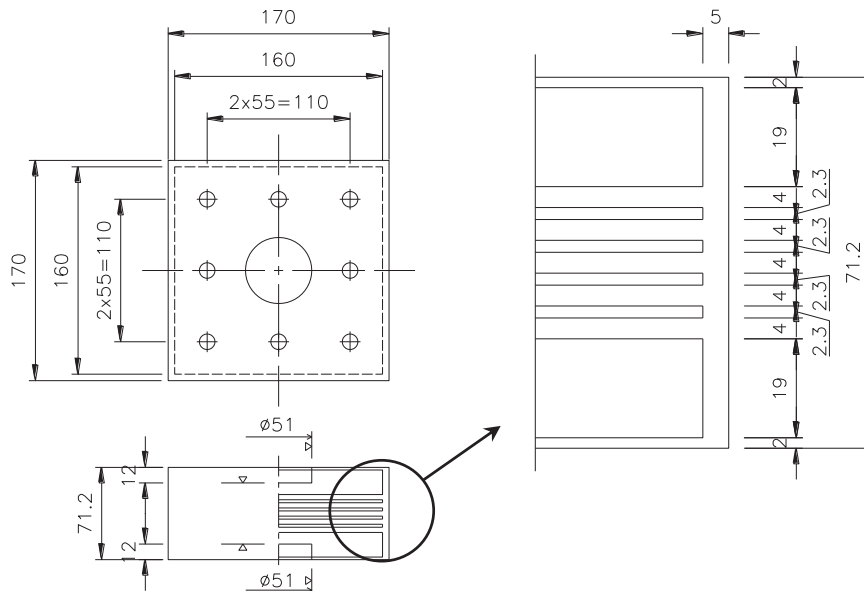


Fig. 3. Size of Type B specimen with smaller dimension [mm] for low temperature tests.

'stress relaxation behavior'. Stress at the end of relaxation period (hold time) can be considered as equilibrium stress whereas the difference between the equilibrium stress and the total stress is

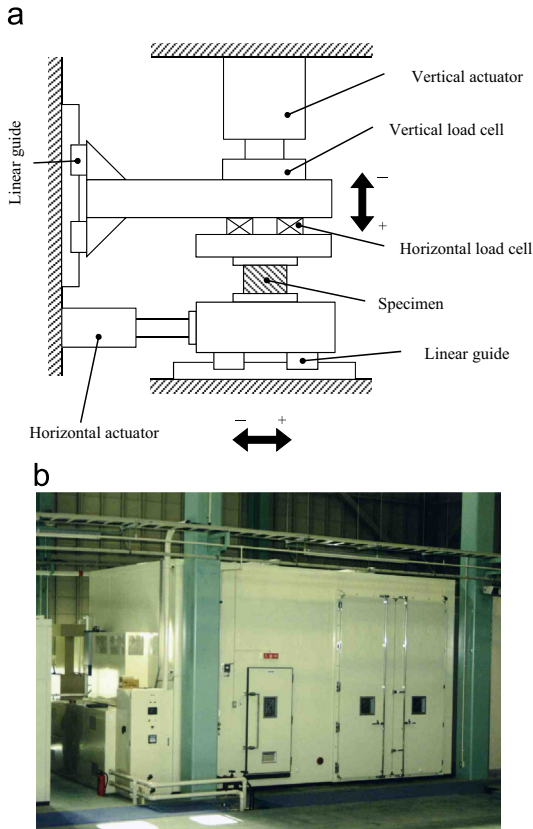


Fig. 4. Test set up. (a) Two axes testing machine. (b) Environmental test chamber for controlling ambient temperature.

Table 2  
Test scheme.

No.	Test name	Specimen type	Test temp. (°C)	Test control parameters						
				Max. shear strain (%)	Test protocol	Strain rate (/s)	Freq. (Hz)	Repetitions	Hold time of each strain (s)	
1	SR100-30 <sup>*</sup>	B	-30	± 100	SR	5.50	–	1	1800	
2	SR150-30 <sup>*</sup>	B	-30	± 150	SR	5.50	–	1	1800	
3	SR175-30 <sup>*</sup>	B	-30	± 175	SR	5.50	–	1	1800	
4	MSR250-30 <sup>*</sup>	B	-30	± 250	MSR	5.50	–	1	1200	
5	Sin175-30 <sup>*</sup>	B	-30	± 175	Sin	< 5.5	0.50	11	–	
6	CS175-30-1.5 <sup>*</sup>	B	-30	± 175	CS	1.50	–	11	–	
7	CS175-30-5.5 <sup>*</sup>	B	-30	± 175	CS	5.50	–	11	–	
8	CS175-30-8.7 <sup>*</sup>	B	-30	± 175	CS	8.75	–	11	–	
9	SR100-10 <sup>*</sup>	B	-10	± 100	SR	5.50	–	1	1800	
10	SR150-10 <sup>*</sup>	B	-10	± 150	SR	5.50	–	1	1800	
11	SR175-10 <sup>*</sup>	B	-10	± 175	SR	5.50	–	1	1800	
12	MSR250-10 <sup>*</sup>	B	-10	± 250	MSR	5.50	–	1	1200	
13	Sin175-10 <sup>*</sup>	B	-10	± 175	Sin	< 5.5	0.50	11	–	
14	CS175-10-1.5 <sup>*</sup>	B	-10	± 175	CS	1.50	–	11	–	
15	CS175-10-5.5 <sup>*</sup>	B	-10	± 175	CS	5.50	–	11	–	
16	CS175-10-8.7 <sup>*</sup>	B	-10	± 175	CS	8.75	–	11	–	
17	SR100-r <sup>#</sup>	A	23	± 100	SR	5.50	–	1	1800	
18	SR150-r <sup>#</sup>	A	23	± 150	SR	5.50	–	1	1800	
19	SR175-r <sup>#</sup>	A	23	± 175	SR	5.50	–	1	1800	
20	MSR250-r <sup>#</sup>	A	23	± 250	MSR	5.50	–	1	1200	
21	Sin175-r <sup>#</sup>	A	23	± 175	Sin	< 11	1.00	11	–	
22	CS175-r-1.5 <sup>#</sup>	A	23	± 175	CS	1.50	–	11	–	
23	CS175-r-5.5 <sup>#</sup>	A	23	± 175	CS	5.50	–	11	–	
24	CS175-r-8.7 <sup>#</sup>	A	23	± 175	CS	8.75	–	11	–	

Source of test data:

\* Current study.

# Bhuiyan et al. [14].

regarded as the 'overstress' due to viscosity induced stress relaxation effect. Closer looks into the stress relaxation behavior observed from SR tests including the stress–strain responses for SR175 tests at three ambient temperatures are presented in Figs. 10–12. All the plots clearly show the relaxation of the stress to be very quick at the first few seconds (Figs. 10(b), 11(b) and 12 (b)) followed by the attainment of an asymptotically converged equilibrium state after few minutes.

Furthermore, in one hand, an inversely proportional general relation between the observed overstress and ambient temperature for each strain level is seen by comparing the recorded stress histories. On the other hand, at a particular ambient temperature, overstress seems to be proportional to the strain applied in the respective SR tests. These are quite in conformity to the earlier observations reported in Amin et al. [11] and Amin et al. [20] for HDR, NR and NR/BR blends. However, the equilibrium states observed that the end of each of the relaxation tests at a particular strain level seems to be much converging irrespective of the ambient temperature, more prominently in the unloading part of the SR tests. Thus equilibrium states were observed here to depend strongly on the current strain but weakly dependent on ambient temperature.

#### 2.5. Cyclic loading tests with constant strain rate (CS) and variable strain rates (Sin) for instantaneous states

Instantaneous response from a solid is the state when the specimen is loaded at an extremely high rate so that the rate dependent part of stress is near to their uppermost limit [9,35]. In practice, high speed simple shear tests or high frequency sinusoidal loading tests are usually used to estimate the instantaneous response of rubber bearings. A series of CS tests were carried out to identify the instantaneous state of HDRBs in this study. As shown in Fig. 6, the strain rate of these tests changes from 1.5/s to 8.75/s with absolute maximum shear strain of 1.75. In addition, the sinusoidal loading tests were conducted using strain

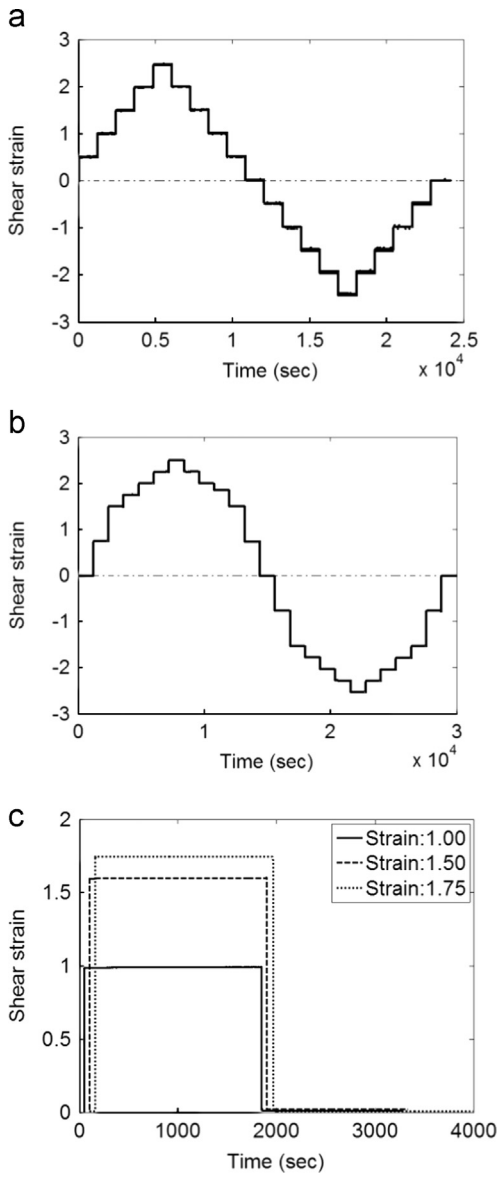


**Fig. 5.** Strain history of MSR and SR tests for (a) MSR tests  $-30\text{ }^{\circ}\text{C}$  &  $-10\text{ }^{\circ}\text{C}$ . (b) MSR tests at  $23\text{ }^{\circ}\text{C}$ . (c) SR tests at  $-30\text{ }^{\circ}\text{C}$ ,  $-10\text{ }^{\circ}\text{C}$  &  $23\text{ }^{\circ}\text{C}$  at 1.00, 1.50 and 1.75 shear strains. The strain histories have been separated by 50 s to each other in (c) for the sake of clarity.

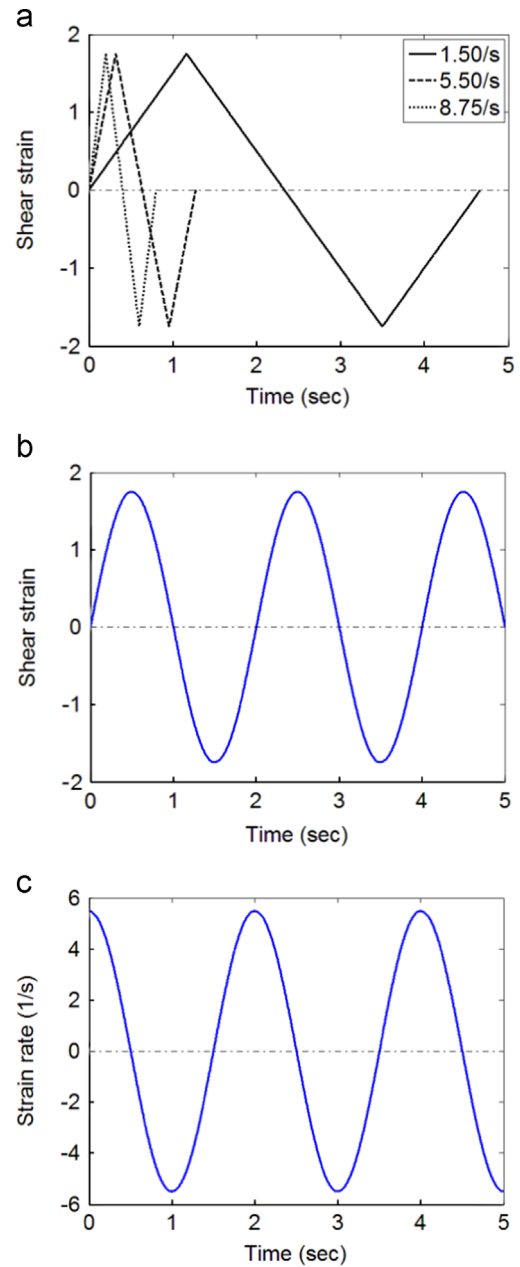


**Fig. 6.** Applied strain histories (a) CS tests at constant strain rate. (b) Sinusoidal (Sin) tests at variable strain rate. (c) Resultant strain rate for sinusoidal tests.

amplitude of 1.75 with a strain rate amplitude of 5.5/s (Fig. 6(c)) to compare with the instantaneous state stress–strain responses obtained from CS tests.

In order to avoid self-heating appearing in the bearing when subjected to cyclic loading, only the 1st cycle of the stress–strain relationship obtained from CS tests is presented and discussed in this section. Fig. 13 shows the 1st cycle of corresponding shear stress–strain relationships of CS tests at different temperatures. The absolute values of maximum stresses are larger than those of minimum stresses in CS tests, especially at low temperatures. These stress-softening behaviors seem to result from the healing of Mullins effect [20,21] occurring with the time lapse between finish of the preloading and start of the actual test. However, the temperature rise inside HDRBs is remarkable at low temperatures [8,36]. This rise also may cause some effect on stress responses in the 1st cycle of CS tests.

It can be observed from Fig. 13 that the stresses become larger in faster loading. However, this stress increase between different loading rates converged at 5.5/s strain rate, since the differences in stresses between strain rates of 5.5/s and 8.75/s are very small. This is in conformity to the experimental observations reported first by Amin et al. [9] on NR and HDR. It implies that the instantaneous state stress–strain relationship of HDRBs can be approximately obtained by loading tests at a rate of 8.75/s. Furthermore, hysteresis exhibited by HDRBs upon cyclic loading, indicated by the areas enclosed by the stress–strain loops, are larger for lower ambient temperatures. Together with the evidences gathered in Sections 2.3 and 2.4 on equilibrium hysteresis and stress relaxation behaviors and their experimentally observed temperature dependence properties, it is apparent that increase in hysteresis as seen in CS and Sin tests at lower ambient

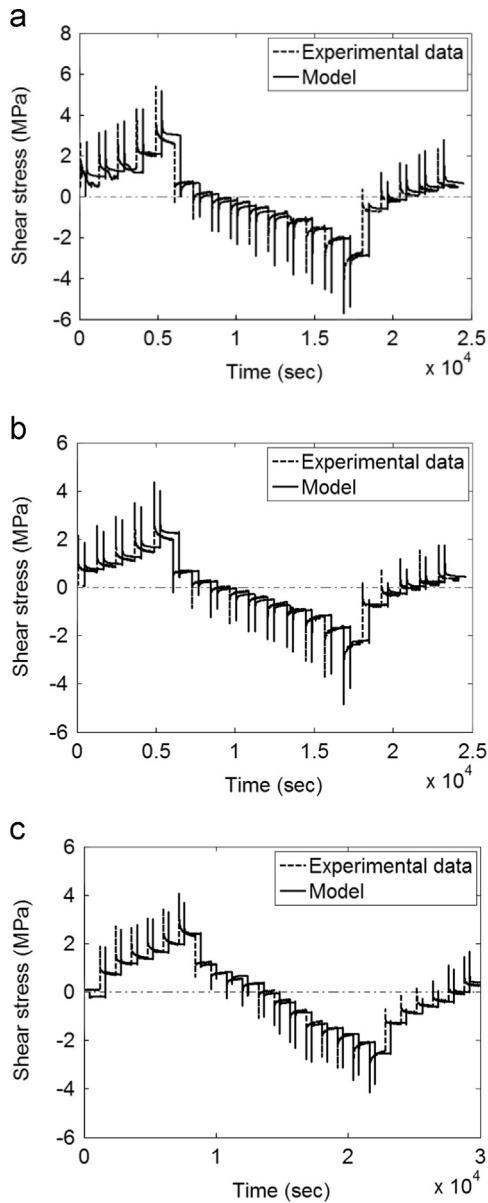


**Fig. 7.** Effect of ambient temperature on stress relaxation behavior observed from MSR tests. Stress histories are shown. (a)  $-30\text{ }^{\circ}\text{C}$ , (b)  $-10\text{ }^{\circ}\text{C}$ , (c)  $23\text{ }^{\circ}\text{C}$ . The stress histories have been separated by 400 s to each other for the sake of clarity.

temperatures are governed primarily by the rate-dependent viscosity properties of HDRBs.

### 3. Rheology model

#### 3.1. Critical observations in experiment and proposed configuration of extended rheology model

The rate dependent behavior of rubber bearing was represented in first attempts by models that separate the total restoring force into rate independent spring and rate dependent dashpot part [13,37]. The total force is approximated as the superposition of spring force and the dashpot damping force. In resemblance with Kelvin model, such models are very straightforward and effective for a few specific loading conditions, though the relaxation tests have already identified hysteresis behaviors that are more complicated to represent in Kelvin model. This limitation has

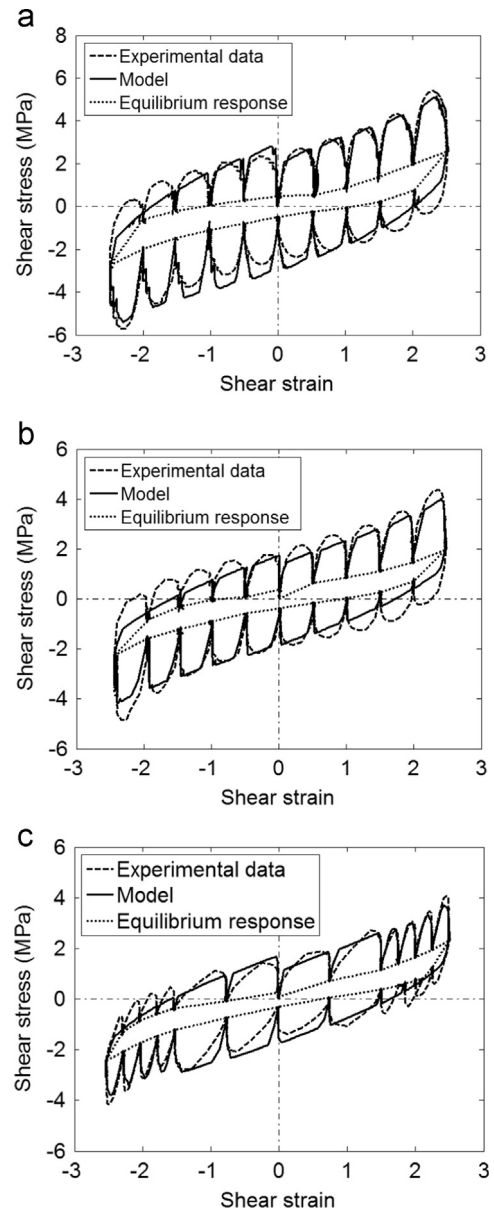


**Fig. 8.** Stress strain responses from MSR tests different temperatures. (a)  $-30\text{ }^{\circ}\text{C}$ , (b)  $-10\text{ }^{\circ}\text{C}$ , (c)  $23\text{ }^{\circ}\text{C}$ .

been improved by the model proposed in Dall'Asta and Ragni [12], where, the rate-dependent behavior was described by two generalized Maxwell elements. Although the HDRBs absorb energy also in a very slow loading rate, the rate-independent part presented by a nonlinear elastic spring in this model cannot represent dissipation of hysteresis energy. Other approaches are presented in the material models of Lion [15], Amin et al. [11] or in the rheology model of Bhuiyan et al. [14]. Commonly, the underlying key approach is an additive decomposition of the total stress into two contributions including rate-independent equilibrium stress and rate-dependent overstress. Even though dilemma hovered around for a long time in identifying the key parameters for these models to effectively represent the hysteresis curves that in reality exists for cyclic dynamic loadings and at the same time also to represent rate dependent behavior as those observed vividly in relaxation tests. Furthermore, most of the previous models were developed from the observations of room temperature tests. Verifications based on low temperature tests are insufficient.

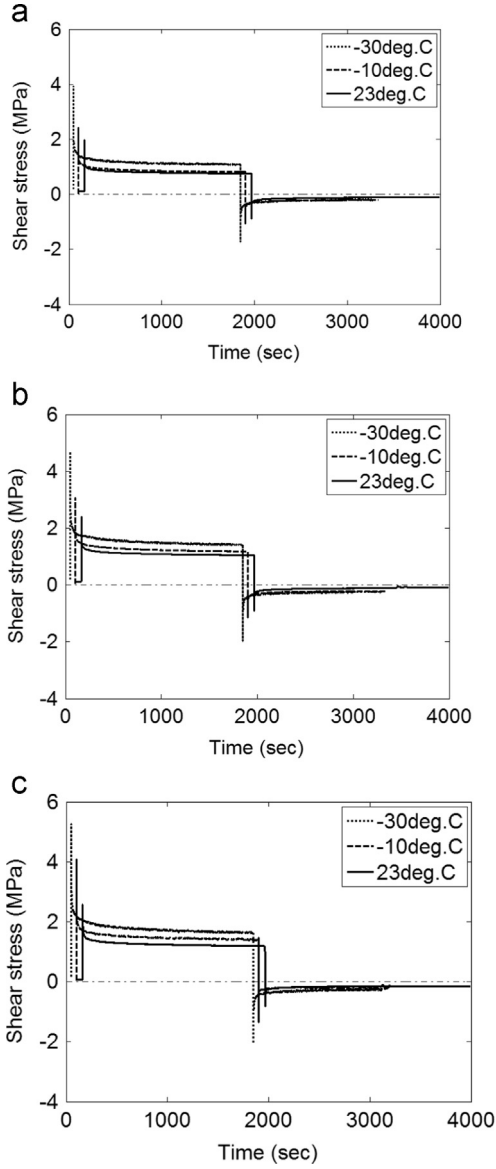


Fig. 9. Effect of ambient temperature on stress relaxation behavior observed from SR tests. Stress histories are shown (a) SR100. (b) SR150. (c) SR175. The stress histories have been separated by 50 s to each other for the sake of clarity.

Based on the original experimental observations (Section 2) reported in this essay, a layout of rheology model is proposed as in Fig. 14. Here, the total stress of HDRBs  $\tau$  is presented as the resultant of rate independent equilibrium stress  $\tau_e$  and rate dependent overstress  $\tau_{oe}$ .

$$\tau = \tau_e + \tau_{oe} \quad (3)$$

As shown in Fig. 14, the equilibrium stress  $\tau_e$  is expressed as three elements: spring  $A_1$ , slider  $S_1$ , and spring  $B_1$ . Spring  $A_1$  is in series with slider  $S_1$ , so that these stresses are equal for each other.

$$\tau_{a1} = \tau_{s1} \quad (4)$$

Meanwhile, spring  $A_1$  and slider  $S_1$  share the total strain as shown in Fig. 14.

$$\gamma = \gamma_{a1} + \gamma_{s1} \quad (5)$$

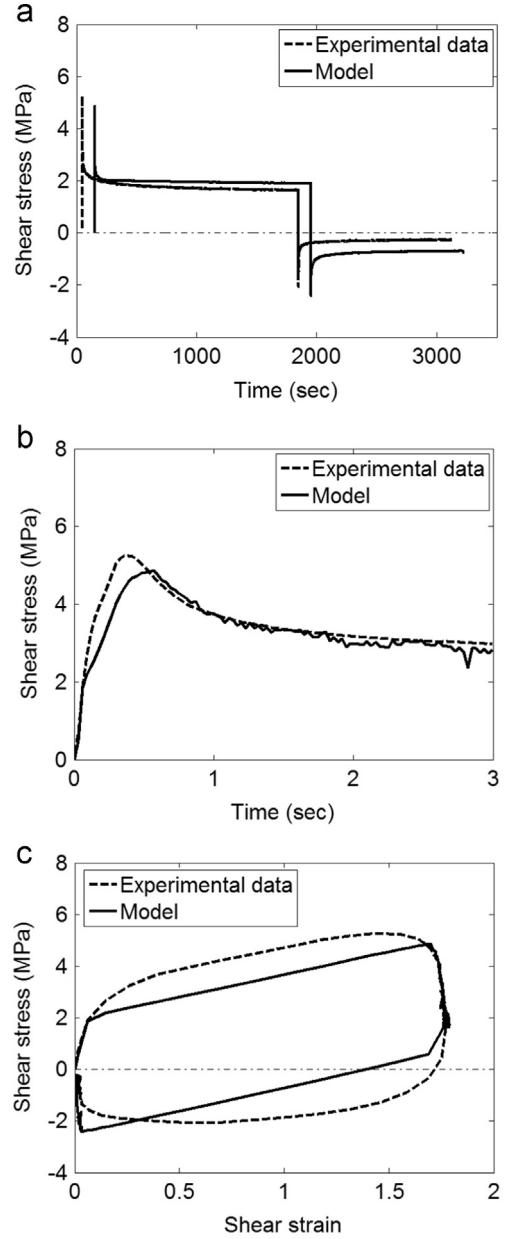


Fig. 10. Responses from SR175 test at  $-30\text{ }^\circ\text{C}$  (a) stress history of the test, (b) close up view of first 3 s, (c) stress–strain response.

Thus, the mentioned elements represent a perfect plastic stress–strain behavior if the spring is linear elastic and the friction force for slider is constant. By combining with spring  $B_1$ , these three elements can be used to simulate bi-linear-model-like behavior with kinematic hardening rule. Equilibrium stress calculated by this numerical model can represent rate independent bilinear model like stress–strain relation, such as those curves observed in MSR tests, as shown in Fig. 8. Accordingly, the equilibrium stress  $\tau_e$  can be calculated as following equation.

$$\tau_e = \tau_{ep} + \tau_{ee} \quad (6)$$

where  $\tau_{ep}$  is the perfect plastic stress in the first branch,  $\tau_{ee}$  is the elastic stress in the second branch. Due to Eqs. (4) and (5), the perfect plastic stress  $\tau_{ep}$  will be altering from elastic state and plastic state.

The instantaneous state boundaries obtained from CS and Sin tests are presented in Section 2.5 (Fig. 13). It is clear from the figures that the initial stiffness is very high, due to well-known Fletcher–Gent effect [38] and also well discussed in Amin et al. [11] for HDR. The second stiffness is lower, however. These aspects can be

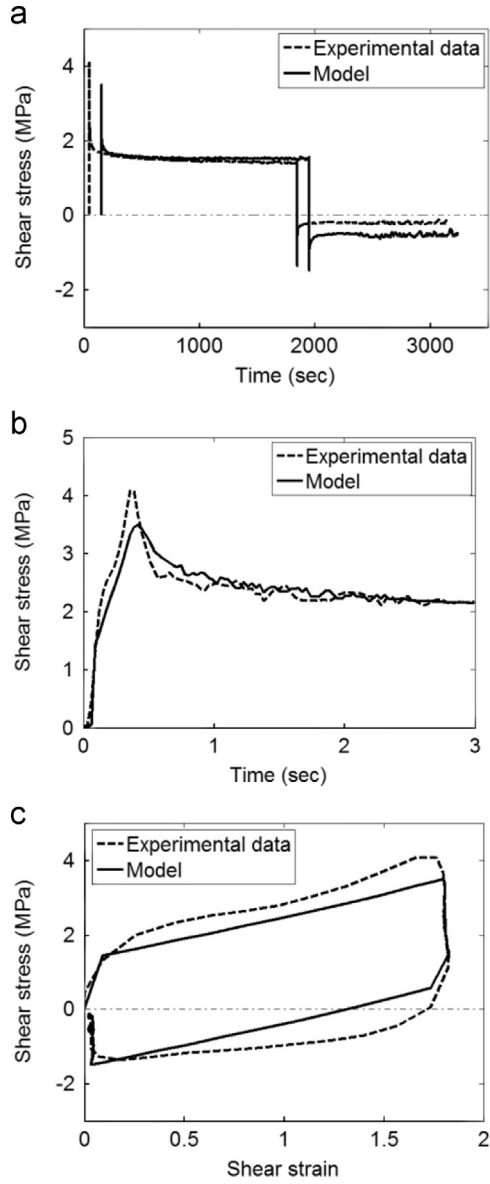


**Fig. 11.** Responses from SR175 test at  $-10\text{ }^{\circ}\text{C}$  (a) stress history of the test, (b) close up view of first 3 s, (c) stress–strain response.

simulated by a bilinear model. Therefore, a structure similar to the equilibrium part is used in the rate dependent overstress part, where the three elements  $A_2$ ,  $S_2$ , and  $B_2$  would represent elasto-plastic behavior, if they were used independently. This elasto-plastic part is connected with a dashpot, as can be seen in Fig. 14, to construct an expanded Maxwell model. This layout for overstress can also be seen as a Maxwell model installed in a nonlinear elasto-plastic spring instead of the original linear elastic spring. Thus, when the bearing is loaded at low strain rate, the overstress is low, Maxwell model performs its relaxation property by letting the dashpot to absorb most of the deformation. On the other hand, when the bearing is loaded at a high strain rate, the deformation of dashpot is locked-up, and the overstress shows bilinear behavior.

### 3.2. Representation of rate-independent equilibrium stress

Stress–strain relationship of spring  $A_1$  is defined as

$$\tau_{ep} = C_1^{(EQ)} \gamma_{a1} \quad (7)$$

where  $C_1^{(EQ)}$  is a constant for spring  $A_1$ .

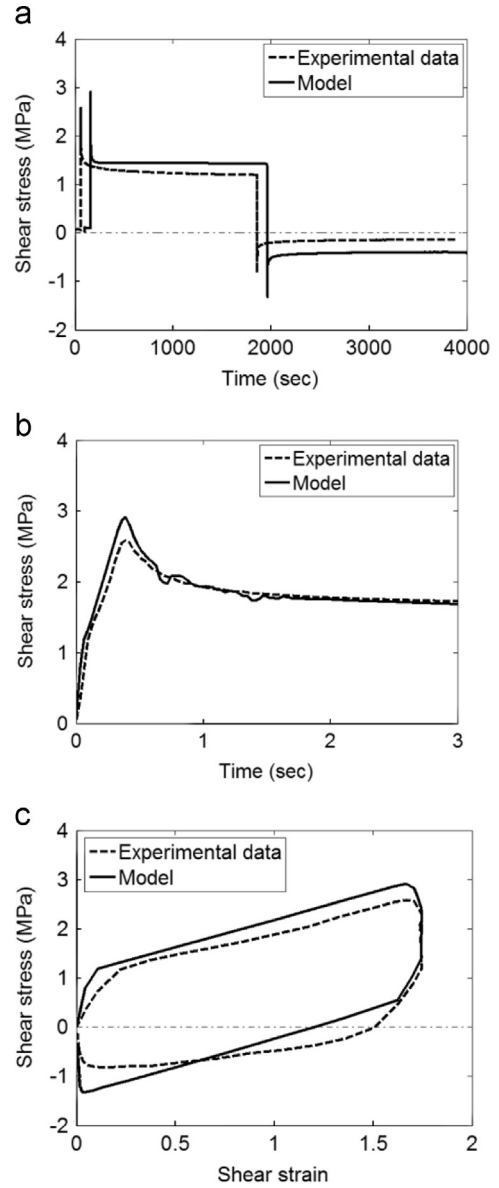


**Fig. 12.** Responses from SR175 test at  $23\text{ }^{\circ}\text{C}$  (a) stress history of the test, (b) close up view of first 3 s, (c) stress–strain response.

Slider  $S_1$  will be activated and start to slide if the stress of spring  $A_1$  reaches the static friction stress  $\tau_{cr}^{(EQ)}$

$$\begin{cases} \dot{\gamma}_{s1} \neq 0 & \text{for } |\tau_{ep}| = \tau_{cr}^{(EQ)} \\ \dot{\gamma}_{s1} = 0 & \text{for } |\tau_{ep}| < \tau_{cr}^{(EQ)} \end{cases} \quad (8)$$

where,  $\tau_{cr}^{(EQ)}$  presents the critical stress of bilinear model, which is defined as the half of the stress difference of hysteresis loop at same strain level. This value also determines the energy dissipation capacity.

Spring  $B_1$  is defined as following nonlinear equation to simulate the experimental observation of the hardening behavior of rubber bearing in large strain domain.

$$\tau_{ee} = C_2^{(EQ)} \gamma + C_3^{(EQ)} |\gamma|^m \text{sgn}(\gamma) \quad (9)$$

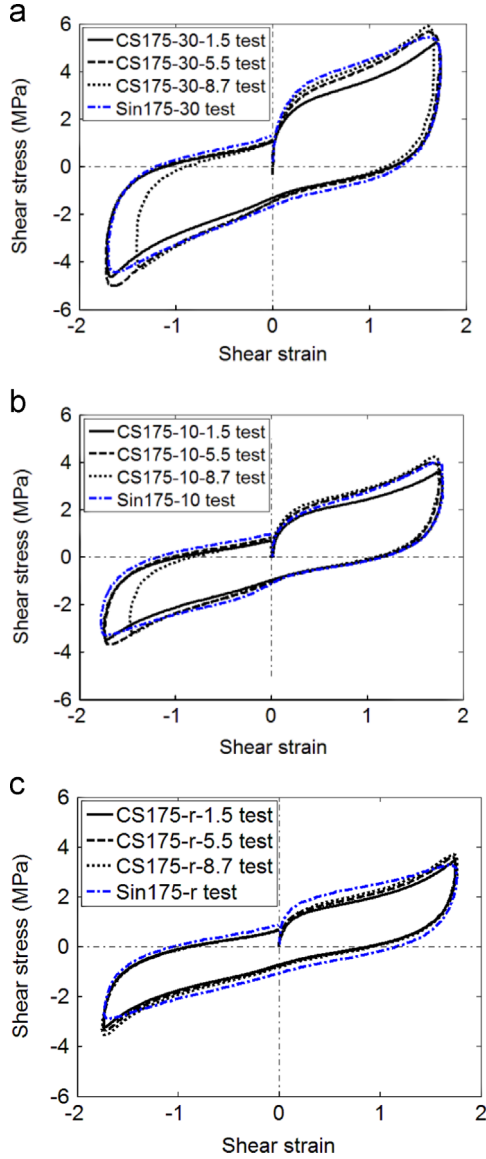


Fig. 13. Shear stress–strain relationships obtained from CS tests at (a)  $-30\text{ }^{\circ}\text{C}$ , (b)  $-10\text{ }^{\circ}\text{C}$ , (c)  $23\text{ }^{\circ}\text{C}$ .

where  $C_2^{(EQ)}$ ,  $C_3^{(EQ)}$ , and  $m$  are parameters and

$$\text{sgn}(x) = \begin{cases} +1 & : x > 0 \\ 0 & : x = 0 \\ -1 & : x < 0 \end{cases} \quad (10)$$

The  $C_1^{(EQ)}$ ,  $C_2^{(EQ)}$ ,  $C_3^{(EQ)}$ ,  $m$  parameters are determined by a standard nonlinear least square method to fit the equilibrium curves obtained by MSR tests (Fig. 8) as illustrated in Fig. 15. The equilibrium parameters as identified at room and low temperatures are listed in Table 3.

### 3.3. Representation of rate-dependent overstress

The overstress in the dashpot  $D$  is equal to the nonlinear elasto-plastic part stress which is logically the sum of the stress  $\tau_a$  in spring  $A_2$  and the stress  $\tau_b$  in spring  $B_2$  as:

$$\tau_{oe} = \tau_a + \tau_b \quad (11)$$

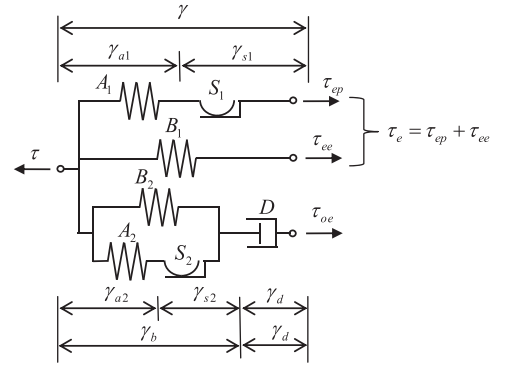


Fig. 14. Configuration of the proposed model.  $\tau$ : average shear stress,  $\gamma$ : average shear strain. Three branches define elasto-plastic stress  $\tau_{ep}$ , nonlinear elastic stress  $\tau_{ee}$  and rate-dependent overstress  $\tau_{oe}$ .

The assumed stress–strain relationships of elements  $A_2$  and  $S_2$  are similar to the relationships of the equilibrium stress.

The stress–strain relationship of spring  $A_2$  is then defined as:

$$\tau_a = C_1^{(OE)} \gamma_{a2} \quad (12)$$

Element  $S_2$  is a friction slider defined as:

$$\begin{cases} \dot{\gamma}_{s2} \neq 0 & \text{for } |\tau_a| = \tau_{cr}^{(OE)} \\ \dot{\gamma}_{s2} = 0 & \text{for } |\tau_a| < \tau_{cr}^{(OE)} \end{cases} \quad (13)$$

The linear stress–strain relationship of spring  $B_2$  can be obtained by following equation:

$$\tau_b = C_2^{(OE)} \gamma_b \quad (14)$$

where  $C_1^{(OE)}$ ,  $\tau_{cr}^{(OE)}$ , and  $C_2^{(OE)}$  are rate dependent overstress parameters.

#### 3.3.1. Viscosity behavior obtained from SR tests

The overstress and dashpot strain rate relationship of element  $D$  in the proposed model is established from SR tests in this section. For this work, the overstress  $\tau_{oe}$  in Eq. (11) is determined from SR tests. The converged stress at the end of each relaxation period is recognized as the equilibrium stress then the overstress is obtained by subtracting the equilibrium stress from the total stress of SR test. Elastic strain  $\gamma_b$  is the solution of Eq. (11), the dashpot strain  $\gamma_d$  can be calculated as  $\gamma_d = \gamma - \gamma_b$  in Fig. 14. The dashpot strain rate is obtained by taking the time derivative of the dashpot strain history. Following this method, the overstress and dashpot strain rate obtained from SR tests are presented in Fig. 16.

Based on the experimental observations presented in Fig. 16, Element  $D$  is assumed to be sub-damping dashpot, so that the stress of  $D$  can be presented by following equation:

$$\tau_{oe} = a \left| \frac{\dot{\gamma}_d}{\dot{\gamma}_0} \right|^n \text{sign}(\dot{\gamma}_d) \quad (15)$$

where  $\dot{\gamma}_0 = 1\text{ (s}^{-1}\text{)}$  is a reference strain rate of the dashpot,  $a$  is the damping coefficient due to viscosity and  $n$  ( $n < 1$ ) is damping exponent. The reference strain rate  $\dot{\gamma}_0$  defines the limit of rate between the domain of slow loading and the domain of fast loading. Loading rate larger than  $\dot{\gamma}_d$  makes  $|\dot{\gamma}_d/\dot{\gamma}_0|$  smaller than one, so that the dashpot outputs a smaller force. In this domain, the system is easier to relax. However, in faster loading over  $\dot{\gamma}_d$  makes the dashpot become easier to be blocked. The overstress parameters are determined from sinusoidal loading tests in the following section.

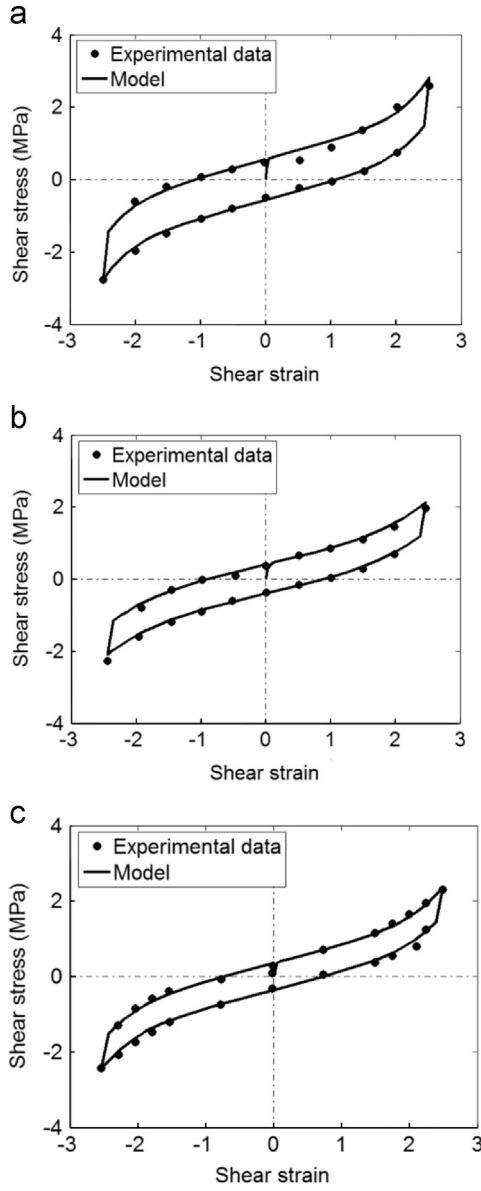


**Fig. 15.** Identification of equilibrium parameters at (a)  $-30\text{ }^{\circ}\text{C}$ , (b)  $-10\text{ }^{\circ}\text{C}$ , (c)  $23\text{ }^{\circ}\text{C}$ .

**Table 3**  
Equilibrium parameters obtained from MSR tests.

Specimen ID	Temperature ( $^{\circ}\text{C}$ )	$C_1^{(EQ)}$ (MPa)	$C_2^{(EQ)}$ (MPa)	$C_3^{(EQ)}$ (MPa)	$\tau_{cr}^{(EQ)}$ (MPa)	$m$
HDR3	$-30$	13.41	0.511	0.0055	0.561	5.62
	$-10$	8.84	0.442	0.0181	0.405	3.94
	23	7.12	0.486	0.0079	0.355	5.03

### 3.3.2. Scheme to identify optimal overstress parameters

In order to determine the overstress parameters,  $C_1^{(OE)}$ ,  $\tau_{cr}^{(OE)}$ ,  $C_2^{(OE)}$ ,  $a$ , and  $n$ ; an optimizing technique is employed. The similarity of numerical result comparing to experimental result is defined here by the following equation:

$$R^2 = 1 - \frac{\sum_{n=1}^N (\tau_{oe}^{\text{exp},n} - \tau_{oe}^{M,n})^2}{\sum_{n=1}^N (\tau_{oe}^{\text{exp},n} - \bar{\tau}_{\text{exp}})^2} \quad (16)$$

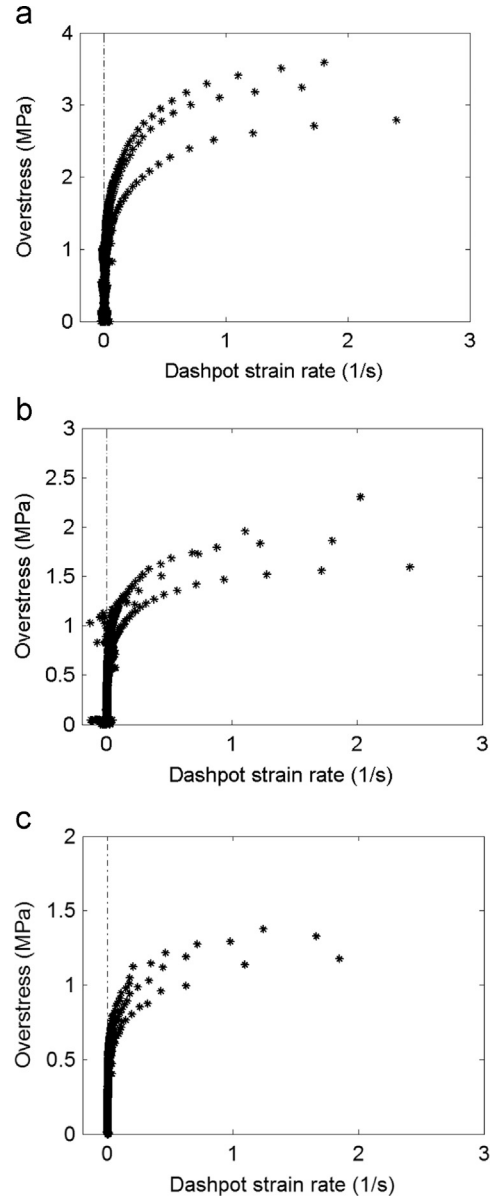


**Fig. 16.** Overstress-dashpot strain rate relationships obtained from SR tests at (a)  $-30\text{ }^{\circ}\text{C}$ , (b)  $-10\text{ }^{\circ}\text{C}$ , (c)  $23\text{ }^{\circ}\text{C}$ .

with

$$\begin{cases} \tau_{oe}^{\text{exp},n} = \tau_{\text{exp},n} - \tau_{\text{eq},n} \\ \bar{\tau}_{\text{exp}} = \frac{\sum_{n=1}^N \tau_{oe}^{\text{exp},n}}{N} \end{cases} \quad (17)$$

where  $N$  is the total number of data points while  $\tau_{oe}^{\text{exp},n}$  and  $\tau_{oe}^{M,n}$  are the overstress obtained from the experiment and the model, respectively, in  $n$  step.  $\bar{\tau}_{\text{exp}}$  is the average value of experimental result.  $\tau_{\text{exp},n}$  and  $\tau_{\text{eq},n}$  are the total shear stress and the equilibrium stress due to experiment, respectively.

Fig. 17 presents the flow chart of the optimizing algorithm. At step 1, the input data include the experimental data, initial values of overstress parameters and values of  $S_l$ ,  $S_r$ ,  $e_{Dl}$ . The step length  $D_i$  is selected to equal 10% of the parameter value at this step. Based on the input data, the stress of the model,  $\tau_M$  and function  $R$  are calculated at step 2. It is important to set the initial values of the parameters to avoid plunging into local optimum solutions. Values of  $C_1^{(OE)}$  and  $C_2^{(OE)}$  can start with the same values of  $C_1^{(EQ)}$  and  $C_2^{(EQ)}$ , respectively. An initial value of  $\tau_{cr}^{(OE)}$  can be obtained by subtracting the value of  $\tau_{cr}^{(OE)}$  from the total stress of the 1st cycle of sinusoidal

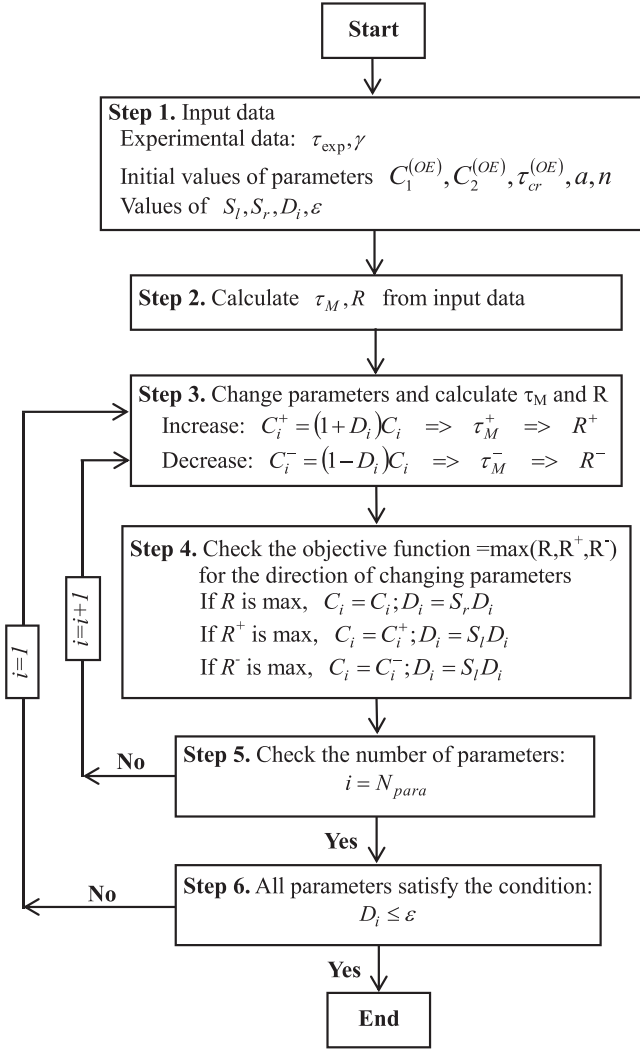


**Fig. 17.** Flow chart to determine the optimal overstress parameters. Notations:  $\tau_{exp}, \gamma$  = the experimental stress and strain, respectively;  $\tau_M$  = the stress obtained from the model;  $C_i$  = the  $i$ th parameter;  $S_l$  = the increasing rate;  $S_r$  = the decreasing rate;  $D_i$  = the step length for parameter  $C_i$ ;  $\epsilon_{D_i}$  = the minimum value of the step rate  $D_i$ ;  $N_{para}$  = the number of overstress parameters.

loading test at the strain level of zero. On the basis of Fig. 16, value of parameter  $n$  should be smaller than one and initial value of  $n$  is selected to equal 0.5. Parameter  $a$  represents the magnitude of the overstress, the initial value can be chosen from 1 MPa to 6 MPa in this calculation.

At step 3, parameter  $C_i$  is varied by Eq. (18) in which  $C_i$  increases by  $D_i C_i$  into  $C_i^+$  and  $C_i$  decreases by  $D_i C_i$  into  $C_i^-$ . Values of  $R^+$  and  $R^-$  can be obtained from  $C_i^+$  and  $C_i^-$  by Eq. (16), respectively.

$$\begin{cases} C_i^+ = (1 + D_i)C_i \\ C_i^- = (1 - D_i)C_i \end{cases} \quad (18)$$

At step 4, the maximum value of  $(R, R^+, R^-)$  is identified to find the optimal direction variation of the parameter. After finding the optimal direction variation of the parameter, the corresponding parameter  $(C, C_i^+, C_i^-)$  is selected and the step length  $D_i$  is

changed by Eq. (19) for the next step  $i + 1$ .

$$\begin{cases} C_i = C_i; D_i = S_r D_i & \text{if } R = \max(R, R^+, R^-) \\ C_i = C_i^+; D_i = S_l D_i & \text{if } R^+ = \max(R, R^+, R^-) \\ C_i = C_i^-; D_i = S_l D_i & \text{if } R^- = \max(R, R^+, R^-) \end{cases} \quad (19)$$

This direct step-by-step iteration of  $C_i$  parameter identification is finished when the optimal condition is satisfied:  $D_i \leq \epsilon_{D_i}$  at step 5 and the optimum program is completed when all parameters are identified at step 6.

In order to minimize the self-heating effect [8,32] on the overstress parameter identification, the 1st cycle shear stress-strain response of sinusoidal loading tests are used in the parameter identification procedure. This assures achieving a thermal boundary condition compatible with the formulation. Fig. 18 shows the identification of overstress parameters by using the optimum program. There is some difference between the experimental and numerical results due to the stress-softening phenomenon occurring in the 1st cycle of sinusoidal loading tests, especially in the hysteresis loops at low temperatures. The model is still calibrated to present the set of experimental result effectively. The optimized parameters are listed in Table 4.

#### 4. Numerical verification

To evaluate the validity of the proposed model, the numerical simulation of MSR tests, CS tests and SR tests as listed in Table 2 were conducted using identified parameters reported in Tables 3 and 4. Though a part of these test data have been used in parameter identification, reversibility and the overall simulation performance need to be checked. Hysteresis curves traced from MSR experiments are traced back via proposed rheology model and plotted in Figs. 7 and 8 against the experimental data points. The stress-strain points obtained from tests and the proposed model at equilibrium state agrees well with each other. It is clearly seen that hysteresis curves generated by the proposed model justifiably represent the rate dependent behavior, such as those local relaxation effects due to holding the strain temporarily and the rising up curve due to the restarted fast loading.

Although all SR tests are simulated to compare with the experiments, due to space limitation, only SR175 simulation results are shown in Figs. 10–12 in comparison to test results. Confident simulation can be observed in all the cases. The simulation results are very close with the experiments at the instantaneous response and the equilibrium state that appear at the beginning and the end of relaxation processes, respectively. The simulations of the relaxation behaviors at the first three seconds of the relaxation processes as compared also matches very closely with the experiments in Figs. 10(b), 11(b) and 12(b). These results show the capability of the proposed model for representing the process-dependent viscosity property of HDRBs.

Though the stress relaxation due to the hold time introduced at the middle of the SR test is rare to occur in real earthquakes acting on a base isolated structure, the low and high speed combined seismic responses from structures are considerable. Furthermore, in some seismic design specifications [25,27] for bridges with HDRBs, a bilinear model is recommended to reproduce the non-linear characteristics of the bearings. The parameters of the bilinear model are determined based on a stress-strain relationship obtained from sinusoidal loading tests with a constant frequency of 0.5 Hz. However, natural frequencies of recent base-isolated bridges vary widely. In particular, base-isolated bridges with sliding bearings, in which HDRBs are often installed as a

stiffness and damping device, have a natural frequency of around 0.2 Hz. In fact, the first and second natural frequencies of Imakirigawa bridge [39], which employs both sliding bearings and HDRBs, are 0.06 and 0.19 Hz, respectively. In those bridges, dominant strain rate of HDRBs under earthquake excitation may become about 20% of that in the sinusoidal loading test with 0.5 Hz frequency. Obviously, the bilinear model base on 0.5 Hz frequency tests is not applicable to these wide range strain-rate problems. The proposed model is intended to simulate wide range of strain-rate behavior of HDRBs, inducing bridges with very small natural frequencies.

Hysteresis curves of HDRBs under CS loading obtained by tests and numerical model analysis are plotted in Fig. 19. Although the target strain level of CS tests is 1.75, the actual strain levels of a few tests are smaller than this value; see the stress response at a strain rate of 8.75/s in Fig. 19(c). The reason may be due to the capability of the test machine, because those test cases require controlling loading history at high load level and fast lading rate. It can be seen that simulation results by the proposed model are close to the experimental results at different strain rates at all the three reference ambient temperatures.

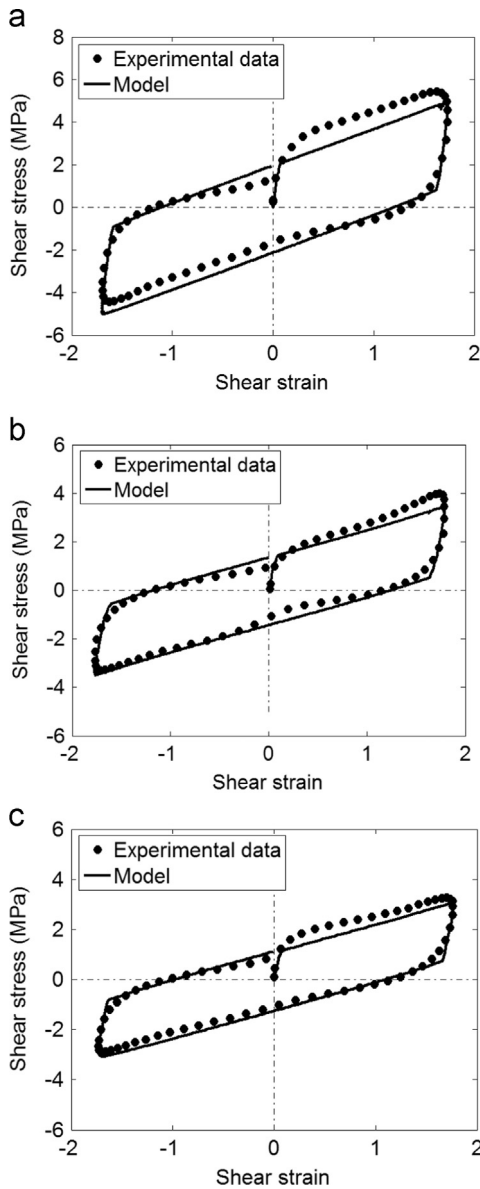


Fig. 18. Identification of overstress parameters at (a) – 30 °C, (b) – 10 °C, (c) 23 °C.

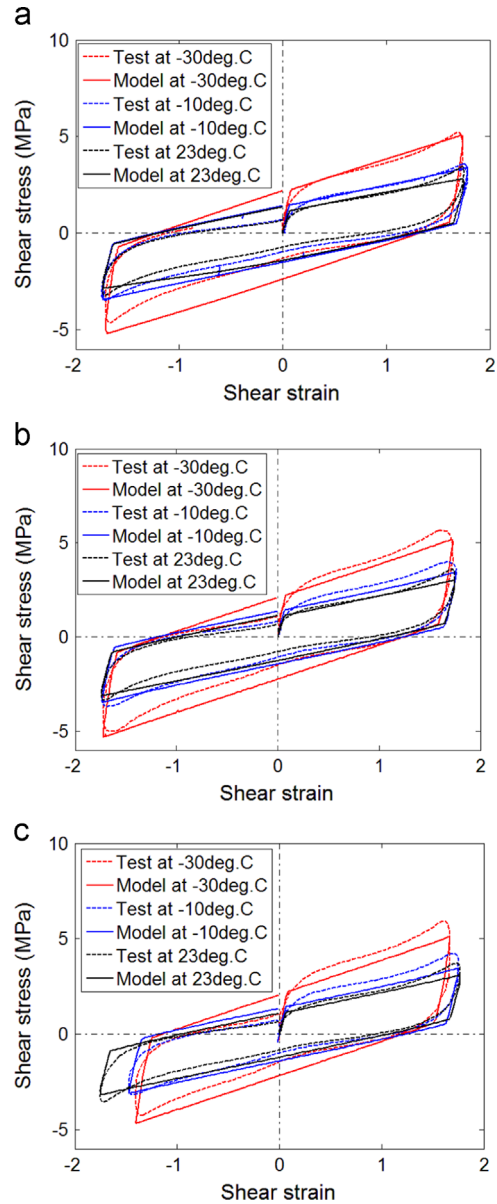


Fig. 19. Numerical simulation of CS175 tests at (a) 1.5/s, (b) 5.5/s, (c) 8.75/s.

Table 4  
Overstress parameters obtained from sinusoidal tests.

Specimen ID	Temperature (°C)	$C_1^{(OE)}$ (MPa)	$C_2^{(OE)}$ (MPa)	$\tau_{cr}^{(OE)}$ (MPa)	$a$ (MPa)	$n$
HDR3	-30	19.17	1.25	1.36	3.93	0.248
	-10	10.36	0.68	0.93	2.53	0.251
	23	10.17	0.65	0.71	1.45	0.238

However, Fig. 19 shows minor discrepancies between experimental and numerical results in terms of energy dissipation and lateral effective stiffness. These discrepancies are presented more clearly by comparing three seismic parameters i.e. energy loss per cycle  $D$ , equivalent damping ratio  $h_{eq}$  and, equivalent shear modulus  $G_{eq}$  defined by

$$h_{eq} = \frac{D}{2\pi W} \quad (20)$$

$$G_{eq} = \frac{\tau_{max} - \tau_{min}}{\gamma_{max} - \gamma_{min}} \quad (21)$$

where  $W$  is the elastic strain energy, which equals the area of the shaded triangle in Fig. 20;  $\tau_{max}$  and  $\tau_{min}$  are the maximum and minimum shear stresses;  $\gamma_{max}$  and  $\gamma_{min}$  are the corresponding shear strains at  $\tau_{max}$  and  $\tau_{min}$ , respectively. The differences between experimental and numerical results are compared in Fig. 21 and Table 5. The differences of the energy loss per cycle and the equivalent damping ratio are quite clear (Fig. 21(a) and (b)), whereas the equivalent shear modulus obtained from numerical results are closely comparable with the modulus obtained from the experimental results (Fig. 21(c)). Such difference also appears in the overstress parameter identification (Fig. 18). The difference between experimental and numerical results seems to be caused by the healing of Mullins effect [20,21] occurring in the time interval between the preloading and the actual test. This situation will not exist when the overstress parameters are determined based on a stress–strain relationship obtained from sinusoidal loading tests after several cycles of loading. In that case, self-heating effect [8,32] should be taken into account. It is the current study of the authors to address self-heating effect. The preliminary result of this topic is presented in [36]. Moreover, the difference between experimental data and simulation results has been discussed in Section 5. However, the ability of the proposed model for representing the rate-dependent behavior induced by viscosity property of HDRBs is verified by the simulations of relaxation tests. This ability remarkably affects the accuracy of the model in predicting the structures' seismic performance with HDRBs, especially in designing isolation structures in seismically active cold areas.

In order to give further evidences to describe the capability of the proposed model in reproducing the rate-dependent behavior of HDRBs, the identified parameters were used in the model to simulate CS responses at low and fast strain rates. Fig. 22 presents simulation results of CS responses at different temperatures. The model has produced logical results in each of the cases, indicating its inherent promises at the design desk.

### 5. Conclusions and final remarks

An experimental test program was carried out to investigate the mechanical behavior of HDRBs at room (23 °C) and low (−30 °C, −10 °C) temperatures under shear deformation with a constant vertical compressive average stress of 6 MPa. Based on

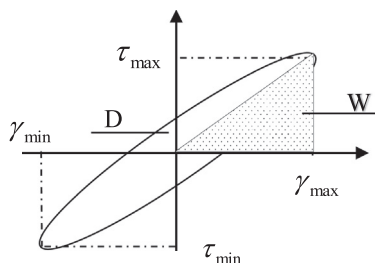


Fig. 20. Hysteresis loop in the stress–strain curve of rubber bearings under cyclic loading.

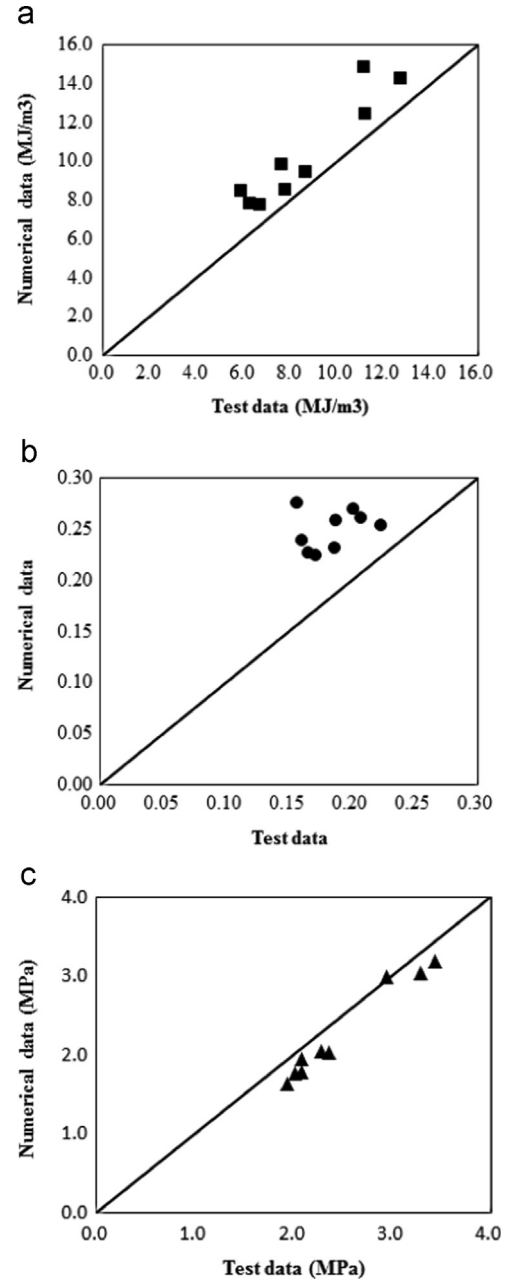


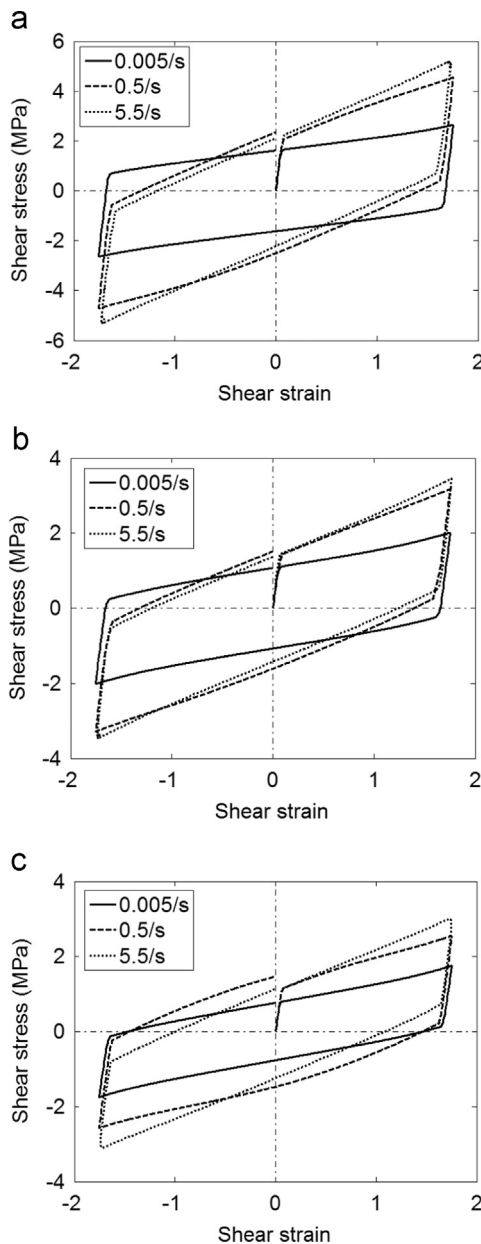
Fig. 21. Comparison between experimental and numerical results (a) dissipated energy per cycle, (b) equivalent damping ratio, (c) equivalent shear modulus.

the experimental results, a rheology model is proposed to describe the mechanical behaviors of HDRBs. The basic layout of the proposed model is considered to present the behavior of HDRBs in rate independent and rate dependent states, equilibrium state and instantaneous state, as observed in test results obtained in the laboratory. Equilibrium parameters are determined from multi-step relaxation tests. The overstress parameters are identified from sinusoidal loading tests by employing an optimal parameter identification method. The model was reasonably successful in simulating fundamental rate dependent cyclic behaviors of HDRBs as vividly observed through experiments under low and room temperatures.

However, a detail comparison between experimental data and simulation results points out the existence of some obvious differences. The differences may arise out due to interference from two other phenomena and their respective temperature history dependences that the rheology model has not taken into account.

**Table 5**Comparison between experimental and numerical results in terms of the energy loss per cycle  $D$ , equivalent damping ratio  $h_B$ , and equivalent shear modulus  $G$ .

Temperature	Strain rate (1/s)	$D$ (MJ/m <sup>3</sup> )		$h_{eq}$		$G_{eq}$ (MPa)		$\Delta D$ (%)	$\Delta h_{eq}$ (%)	$\Delta G_{eq}$ (%)
		Test	Model	Test	Model	Test	Model			
−30 °C	1.5	11.1	14.8	0.20	0.27	2.94	2.99	24.9	25.2	1.88
	5.5	12.7	14.3	0.22	0.25	3.28	3.05	10.7	12.2	7.20
	8.75	11.2	12.4	0.19	0.23	3.43	3.19	9.83	19.5	7.04
−10 °C	1.5	7.61	9.80	0.19	0.26	2.08	1.95	22.4	27.2	6.20
	5.5	8.67	9.41	0.21	0.26	2.28	2.04	7.82	20.4	10.2
	8.75	7.79	8.53	0.17	0.22	2.36	2.04	8.64	23.6	13.6
23 °C	1.5	5.87	8.42	0.16	0.28	1.93	1.64	30.3	43.1	15.1
	5.5	6.28	7.80	0.16	0.24	2.02	1.77	19.6	32.7	12.1
	8.75	6.72	7.73	0.17	0.23	2.08	1.79	13.1	26.8	14.1

**Fig. 22.** Shear stress–strain relationships obtained from numerical simulation of CS175 tests at (a) −30 °C, (b) −10 °C, (c) 23 °C.

These are the healing of Mullins softening effect [12,20,21] and the self-heating effect [22,23,32]. The first phenomenon increases the hysteresis, whereas the second one tends to reduce it. As final

remarks, it is to emphasize that healing of Mullins effect, self-heating effect and their respective temperature history dependences should also be considered carefully to more accurately simulate the performances of structures isolated with HDRBs but located in seismically active cold regions.

### Acknowledgements

The experimental works were conducted by utilizing the laboratory facilities and bearings-specimens provided by Japan Rubber Bearing Association. The authors indeed gratefully acknowledge the kind cooperation extended by them in performing the tests according to the test plans of the authors. This work was supported by JSPS KAKENHI (Grants-in-Aid for Scientific Research) Grant number 26289140.

### References

- [1] Kelly JM. Earthquake-resistant design with rubber. 2nd ed.. London: Springer-Verlag; 1997.
- [2] Kumar M, Whittaker AS, Constantinou MC. An advanced numerical model of elastomeric seismic isolation bearings. *Earthquake Eng Struct Dyn* 2014;43(13):1955–74.
- [3] Robinson WH. Lead rubber hysteretic bearings suitable for protecting structures during earthquakes. *Earthquake Eng Struct Dyn* 1982;10(4):593–604.
- [4] Skinner RI, Robinson WH, Mc Verry GH. An introduction to seismic isolation. England: John Wiley and Sons; 1993.
- [5] Kalpakidis I, Constantinou M. Effects of heating on the behavior of lead-rubber bearings. I: Theory. *J Struct Eng ASCE* 2009;135(12):1440–9.
- [6] Kalpakidis I, Constantinou M. Effects of heating on the behavior of lead-rubber bearings. II: Verification of theory. *J Struct Eng ASCE* 2009;135(12):1450–61.
- [7] Razzaq MK, Okui Y, Bhuiyan AR, Amin A, Mitamura H, Imai T. Application of rheology modeling to natural rubber and lead rubber bearings: a simplified model and low temperature behavior. *Struct Eng/Earthquake Eng JSCE* 2012;29(2):40–55.
- [8] Cardone D, Gesualdi G, Nigro D. Effects of air temperature on the cyclic behavior of elastomeric seismic isolators. *Bull Earthquake Eng* 2011;9(4):1227–55.
- [9] AFMS Amin, Alam MS, Okui Y. An improved hyperelasticity relation in modeling viscoelasticity response of natural and high damping rubbers in compression: experiments, parameter identification and numerical verification. *Mech Mater* 2002;34:75–95.
- [10] Amin AFMS, Wiraguna SI, Bhuiyan AR, Okui Y. Hyperelasticity model for finite element analysis of natural and high damping rubbers in compression and shear. *J Eng Mech ASCE* 2006;132(1):54–64.
- [11] Amin AFMS, Lion A, Sekita S, Okui Y. Nonlinear dependence of viscosity in modeling rate-dependent response of natural and high damping rubbers in compression and shear: experimental identification and numerical verification. *Int J Plast* 2006;22:1610–57.
- [12] Dall'Asta A, Ragni L. Experimental tests and analytical model of high damping rubber dissipating devices. *Eng Struct* 2006;28:1874–84.
- [13] Hwang JS, Wu JD, Pan TC, Yang G. A mathematical hysteretic model for elastomeric isolation bearings. *Earthquake Eng Struct Dyn* 2002;31:771–89.
- [14] Bhuiyan AR, Okui Y, Mitamura H, Imai T. A rheology model of high damping rubber bearings for seismic analysis: identification of nonlinear viscosity. *Int J Solids Struct* 2009;46:1778–92.

- [15] Lion A. A constitutive model for carbon black filled rubber: experimental investigations and mathematical representation. *Continuum Mech Thermodyn* 1996;8:153–69.
- [16] Yamamoto M, Minewaki S, Yoneda H, Higashino M. Nonlinear behavior of high-damping rubber bearings under horizontal bidirectional loading: full-scale tests and analytical modeling. *Earthquake Eng Struct Dyn* 2012;41(13):1845–60.
- [17] Kato H, Mori T, Murota N, Kikuchi M. Analytical model for elastoplastic and creep-Like behavior of high-damping rubber bearings. *J Struct Eng ASCE* 2014. [http://dx.doi.org/10.1061/\(ASCE\)ST.1943-541X.0001181](http://dx.doi.org/10.1061/(ASCE)ST.1943-541X.0001181).
- [18] Lion A. On the large deformation behavior of reinforced rubber at different temperatures. *J Mech Phys Solids* 1997;45:1805–34.
- [19] Fuller KNG, Gough J, Thomas AG. The effect of low-temperature crystallization on the mechanical behavior of rubber. *J Polym Sci Part B: Polym Phys* 2004;42(11):2181–90.
- [20] Amin AFMS Lion A, Höfer P. Effect of temperature history on the mechanical behaviour of a filler-reinforced NR/BR blend: literature review and critical experiments. *ZAMM-J Appl Math Mech/Z Angew Math Mech* 2010;90(5):347–69.
- [21] Mullins L. Softening of rubber by deformation. *Rubber Chem Technol* 1969;42:339–62.
- [22] Gent AN, Hindi M. Heat build-up and blowout of rubber blocks. *Rubber Chem Technol* 1988;61(5):892–905.
- [23] Park DM, Hong WH, Kim SG, Kim HJ. Heat generation of filled rubber vulcanizates and its relationship with vulcanizate network structures. *Eur Polym J* 2000;36(11):2429–36.
- [24] Yakut A, Yura JA. Parameters influencing performance of elastomeric bearings at low temperatures. *J Struct Eng ASCE* 2002;128:986–94.
- [25] American association of state highways and transportation officials (AASHTO). Guide specification for seismic isolation design. 3rd ed. Washington DC; 2010.
- [26] Japan road association (JRA). Specifications for highway bridges. Part V: Seismic design. Tokyo: Maruzen; 1996.
- [27] Japan road association (JRA). Specifications for highway bridges. Part V: Seismic design. Tokyo: Maruzen; 2002.
- [28] Japan road association (JRA). Bearing support design guide for highway bridges (in Japanese). Japan; 2012.
- [29] Imai T, Satoh T, Nishimura T, Tanaka H, Mitamura H. The performance evaluations of rubber bearings for bridges in cold districts (in Japanese). In: Proceedings of the 64th conference of Hokkaido Branch of JSCE, Japan; 2008. p. A-18.
- [30] Bhuiyan AR. Rheology modeling of laminated rubber bearings for seismic analysis. Japan: Dissertation, Saitama University; 2009.
- [31] International organization of standardization (ISO). Elastomeric seismic protection isolators. Part 1: Test methods; 2005.
- [32] Takaoka E, Takenaka Y, Kondo A, Hikita M, Kitamura H. Heat-mechanics interaction behavior of laminated rubber bearings under large and cyclic lateral deformation. In: Proceedings of the 14th world conference on earthquake engineering, Beijing, China; 2008. p. 12–17.
- [33] Research committee of isolation structure in road bridges. Collection of examples of isolated bridges in Japan (in Japanese). Tokyo: Public Works Research Center; 2011.
- [34] Miehe C, Keck J. Superimposed finite elastic-viscoelastic-plastoelastic stress response with damage in filled rubbery polymers. Experiments, modeling and algorithmic implementation. *J Mech Phys Solids* 2000;48:323–65.
- [35] Huber N, Tsakmakis C. Finite deformation viscoelasticity laws. *Mech Mater* 2000;32:1–18.
- [36] Nguyen DA, Okui Y, Hasan MD, Mitamura H, Imai T. Mechanical behavior of high damping rubber bearings at low temperatures. In: Proceedings of the 12th international symposium on new technologies for urban safety of mega cities in Asia, Hanoi Vietnam; 2013. p. 1067-74.
- [37] Tsai CS, Tsu-Cheng Chiang, Bo-Jen Chen, Shih-Bin Lin. An advanced analytical model for high damping rubber bearings. *Earthquake Eng Struct Dyn* 2003;32:1373–87.
- [38] Fletcher WP, Gent AN. Non-linearity in the dynamic properties of vulcanized rubber compounds. *Trans Inst Rubber Ind* 1953;29:266–80.
- [39] Matsuda T, Igarashi A, Furukawa A, Ouchi H, Uno H, Matsuda H. Effect of inter-component phase difference in bi-directional seismic ground motion input to dynamic response of ICSS (in Japanese). *J JSCE, Ser A1 (Struct Eng & Earthquake Eng (SE/EE))* 2013;69(2):688–702.